Kinetics and Mechanism of Steady-State Catalytic NO Decomposition Reactions on Cu–ZSM5

Björn Modén, Patrick Da Costa, Benjamin Fonfé, Deuk Ki Lee,[1] and Enrique Iglesia[2]

Department of Chemical Engineering, University of California at Berkeley, Berkeley, California 94720

A sequence of elementary steps for the formation of N_2O, NO_2, N_2, and O_2 during NO decomposition on Cu–ZSM5 was inferred from steady-state and transient rate data combined with previous spectroscopic evidence for adsorbed species and Cu structures. Transient product evolution rates confirmed the redox nature of this sequence and the role of Cu dimers with labile oxygen atoms. N_2O formed near ambient temperature as the initial decomposition product after quasiequilibrated adsorption of NO on reduced Cu^+ dimers. The low activation energy for this step, the significant heat of adsorption of NO on Cu^+ dimers, and the transition in prevalent Cu structures from $\{Cu^{2+}–O^{2-}–Cu^{2+}\}^{2+}$ to $\{Cu^+–\square–Cu^+\}^{2+}$ lead to the observed decrease in NO decomposition rates above 750 K. Quasiequilibrium between O_2 and $\{Cu^{2+}–O^{2-}–Cu^{2+}\}^{2+}$ is mediated by a set of steps involving NO_2 formation and decomposition, which lead to equilibrium NO_2 concentrations during NO decomposition at 650–850 K on Cu–ZSM5. These pathways are faster than recombinative desorption steps requiring vicinal Cu^{2+} dimers with labile oxygen atoms to form O_2. In these steps, NO acts as a regenerable oxygen carrier that allows kinetic communication among remote adsorbed oxygen atoms via diffusion in the gas phase. Rate equations for the decomposition of NO and for product formation and the temperature dependence of their rate parameters are consistent with the kinetic data reported and with the effects of temperature on the relative abundance of adsorbed species and of Cu structures. These elementary steps suggest that redox steps restricted to Cu^{2+} and Cu^+ cycles, the presence of vicinal Cu atoms to accommodate two adsorbed NO molecules and a two-electron reduction without the formation and agglomeration of Cu metal, and the balanced equilibrium between $\{Cu^{2+}–O^{2-}–Cu^{2+}\}^{2+}$ and $\{Cu^+–\square–Cu^+\}^{2+}$ species account for the high NO decomposition rates achieved on Cu–ZSM5 catalysts.   © 2002 Elsevier Science (USA)

Key Words: NO decomposition; kinetics; Cu–ZSM5; redox mechanism; copper dimers; temperature effect.

INTRODUCTION

Nitrogen oxides (NO and NO_2) form in combustion processes and lead to local high ozone concentrations and to acid rain. Catalytic reduction processes using NH_3 or traces of residual hydrocarbons are currently used in order to reduce N_2O, NO, and NO_2 concentrations in combustion-effluent streams (1, 2). Such processes become more challenging as lean-burn strategies are used to increase energy efficiency. The catalytic decomposition of NO is favored by thermodynamics at typical effluent conditions and this reaction does not require a reductant (3). Reported catalytic NO decomposition rates, however, remain too low for practical applications.

Cu-exchanged pentasil zeolites (Cu–ZSM5) are among the most active NO decomposition catalysts reported (4–8). Cu dimers bridging two exchange sites have been proposed as active sites for NO decomposition (8–11, 16); the bridging oxygens in such dimers provide redox sites required for catalytic turnovers. Liu and Robota (12) reported a parallel increase in NO decomposition rates and in the number of Cu^+ species detected by X-ray absorption spectroscopy during reaction at temperatures up to 773 K. These data suggested that turnovers involve cycling between Cu^+ and Cu^{2+} states and that NO adsorption occurs on Cu^+ cations, which oxidize by abstracting oxygen from adsorbed NO. Infrared spectroscopy has been used to probe interactions between NO and Cu ions (Cu^+ and Cu^{2+}) in ZSM5 (8, 9, 13–23). The detection of a band for $Cu^+(NO)$ confirmed the proposal that Cu^+ adsorbs NO (17, 20, 21) as well as the kinetic relevance of Cu^+/Cu^{2+} cycles (17). Various adsorbed NO_x species have been proposed as intermediates leading to the formation of O_2, among others a bridging nitrate species $\{Cu^{2+}–(NO_3^-)–Cu^{2+}\}$ (20).

Cu dimers that cycle between Cu^+ and Cu^{2+} during each NO decomposition turnover (8, 11) coexist with isolated Cu^{2+} sites anchored at two exchange sites and with Cu oxides (Cu_2O, CuO) (9, 24). In the experiments reported in the current study, Cu–ZSM5 samples contain predominately $\{Cu^{2+}–O^{2-}–Cu^{2+}\}^{2+}$ and Cu^{2+} species, each interacting with two exchange sites (10). No CuO structures were evident from the kinetics and stoichiometry of their reduction in H_2 or CO, which were used in order to probe the speciation of Cu^{2+} species in these samples (10).

NO decomposition rate equations have been reported on several metal and metal oxide surfaces. NO concentration

---

orders are between 1 and 2 and reaction orders in O_2 vary between -1 and -0.5 (25–28). A first-order NO dependence on Pt led to the proposal that the initial adsorption of NO on Pt is the kinetically relevant step (26–28) and mobile chemisorbed oxygen atoms were invoked in order to explain the -1 order in O_2. NO decomposition rate studies on Ba/MgO (29), $La_{0.8}Sr_{0.2}CoO_3$ and $La_{0.4}Sr_{0.6}Mn_{0.8}Ni_{0.2}O_3$ (30), and Mn_2O_3 and Mn_3O_4 (31) have shown a second-order NO dependence. On metal oxides, oxygen vacancies are thought to provide the active sites for the adsorption of NO, in the first step of redox NO decomposition cycles (32).

Several NO decomposition rate studies on Cu–ZSM5 have been reported (4, 5, 33–37). Li and Hall proposed a power-law equation with a first-order NO dependence and a -0.5 order in O_2 (34). These orders varied with temperature; the O_2 dependence became weaker and the NO dependence increased slightly with increasing temperature. NO decomposition rates increased with temperature up to 773 K and then decreased at higher temperatures (4, 5, 34). Li and Hall (34) suggested that NO adsorption becomes unfavorable as temperature increases, leading to a decrease in the concentration of these intermediates at higher temperatures. In contrast, NO decomposition rates on Pt catalysts showed a normal Arrhenius dependence and increased monotonically with increasing temperature (26; see also Fig. 9).

This study aims to combine recent spectroscopic findings about the nature of reactive intermediates with transient kinetic measurements (11) into a mechanism consistent with measured rates for NO decomposition and for NO_2, N_2O, O_2, and N_2 formation. The elementary steps proposed include specific pathways for the removal of adsorbed oxygen; these steps avoid the previously proposed recombinative desorption steps, which are difficult to reconcile with the isolated nature of oxygen atoms in Cu dimers. Finally, the steps proposed incorporate the formation of N_2O and NO_2 into an overall mechanism of NO reactions in the presence of O_2. This set of elementary steps is consistent with steady-state rate data and with available spectroscopic and transient data reported elsewhere.

EXPERIMENTAL SECTION

Catalyst Synthesis and Characterization

Cu–ZSM5 samples were prepared by ion exchange of Cu^{2+} ions into Na–ZSM5 zeolite (Zeochem, 10 g; two batches with Si/Al = 14.7 and 13.3) using 0.01–0.1 M copper acetate solutions (1 liter, $Cu(CH_3COO)_2$ H_2O, Sigma Aldrich, ACS reagent) in doubly deionized water. Ion exchange was carried out for 20 h at ambient temperature. These samples were then rinsed six times using 300-cm³ batches of doubly deionized water with filtering between rinsing steps. For some samples, this exchange procedure

TABLE 1

Composition of Cu–ZSM5 Catalysts and N_2 Formation Rates Obtained for the Steady-State NO Decomposition Reaction

Catalyst					
Cu (wt%)	0.76	2.24	2.25	3.31	3.88
Si/Al (atomic ratio)	13.3	14.6	13.1	14.3	13.2
Cu/Al (atomic ratio)	0.12	0.38	0.36	0.58	0.60
N_2 Formation Rate[a]					
μmol N_2 (g catalyst)$^{-1}$ s^{-1}	0.067	1.66	1.41	3.35	4.08
10^3 mol N_2 (mol Cu)$^{-1}$ s^{-1}	0.56	4.71	3.98	6.42	6.64

[a] Measured at 773 K, 0.05 g catalyst, 1.0 cm³ s^{-1} flow rate, and 1 kPa NO. Extrapolated to zero conversion (1 kPa NO, 0 kPa O_2) using Eq. [13].

was repeated in order to achieve higher Cu exchange levels. The samples were then dried in ambient air at 383 K for 24 h, pelleted, crushed, and sieved to retain agglomerates with 125- to 250-μm diameters. The Si, Al, and Cu concentrations were measured by ion-coupled plasma emission spectroscopy (Galbraith Laboratories) (Table 1). All Cu–ZSM5 samples are labeled Cu(x), where x is the atomic Cu/Al ratio. More-detailed characterization of these catalysts is presented elsewhere (10). A Pt/Al$_2$O$_3$ catalyst (5 wt%; Alfa–Aesar) was used as a comparison with Cu–ZSM5. The titration of adsorbed oxygen by H_2 at 373 K was used to measure a Pt dispersion of 29%. All catalysts were treated in He at 773 K for 2 h before NO decomposition kinetic experiments.

Steady-State NO Decomposition Rate Measurements

NO, He, O_2, NO_2, and a calibration gas mixture were used in NO decomposition kinetic measurements. The NO mixture was supplied by Matheson as 1.00% NO, 9.98% Ar, and 89.02% He (<10 ppm other gases). Helium (UHP grade, Bay Airgas) was used for catalyst pretreatment and for dilution of the 1.00% NO mixture to lower NO concentrations. The O_2 mixture contained 4.99% O_2 and 95.01% He (Praxair). The NO_2 mixture contained 0.05% NO_2, 10% Ar, and 89.95% He (Praxair). The calibration gas contained 0.05% N_2, 0.05% O_2, 0.05% N_2O, 10% Ar, and 89.85% He (Praxair).

The reactant and effluent streams were analyzed using an online mass spectrometer (MKS Instruments, Orion Compact Residual Gas Analyzer) differentially pumped in order to sample streams at ambient pressure without mass discrimination (Pfeiffer, vaccum system TCP015). The Ar present in the NO reactant mixture was used as an internal standard in measuring the concentrations of NO, N_2, N_2O, O_2, and NO_2. Calibration factors for N_2 (28 amu), N_2O (44 amu), and O_2 (32 amu) relative to Ar (40 amu) were obtained from ion yields measured using the calibration mixtures. NO and NO_2 calibrations were obtained from NO (30 amu) and NO_2 (46 amu) ion yields using the NO and NO_2 reactant mixtures.

Steady-state NO decomposition rates were measured using a quartz microreactor (18-mm inner diameter) with the catalyst samples supported on a porous quartz frit. The catalyst bed contained 50-mg samples with a bed height of <5 particle diameters; this shallow bed allows reaction rate descriptions using the formalism applicable to well-mixed flow reactors (38). All experiments were carried out at ambient total pressure. Bed temperatures were measured using a type K thermocouple affixed to the outer reactor surface. The temperature was maintained using an electronic controller (Watlow, Series 988) and a resistively heated furnace (National Element, Type FA 120, 360 W). Each of the gas mixtures was metered using calibrated electronic mass flow controllers (Porter Instruments, Model 201).

The overall NO molar decomposition rate is twice the combined molar formation rates of N_2O and N_2. Throughout this manuscript, we use the sum of the formation rates of N_2 and N_2O as a measure of the rate of the reaction. Steady-state $N_2 + N_2O$ formation rates [mol $(N_2 + N_2O)$ (mol Cu)$^{-1}$ s^{-1}] were compared with mechanism-derived rate expressions using least-squares methods (39, 40). The regression analysis minimized the sum of the square of the relative deviations for all data points. Rate data were obtained over a range of NO pressures (0.2–1 kPa), O_2 pressures (0–1 kPa), and contact times (10–60 ms) at three reaction temperatures (723, 773, and 823 K).

Temperature-Programmed and Isothermal Transient Experiments

In temperature-programmed experiments, samples were treated in 50% O_2/He at 773 K for 2 h. Then, the temperature was decreased to 298 K and He was introduced in order to remove weakly adsorbed O_2. The temperature was then increased in either He or 0.464% NO/He streams in order to probe O_2 formation pathways in the presence and absence of NO. During steady-state NO decomposition experiments, rapid isothermal transients were performed between NO-containing streams and He. The details of these temperature-programmed and isothermal transient experiments are reported elsewhere (11).

RESULTS AND DISCUSSION

NO conversion to N_2O initially increased with contact time, but ultimately decreased, as N_2O decomposed further to form N_2 and O_2 (Fig. 1). This behavior is typical of sequential reactions and it indicates that N_2O acts as an intermediate in the decomposition of NO to N_2 and O_2 on Cu–ZSM5. Thus, N_2 formation proceeds via the sequence NO → N_2O → N_2. Below 723 K, N_2O is detected at all contact times, but N_2 becomes the only detectable nitrogen-containing product at higher temperatures (Fig. 2). This implies that N_2O decomposition rate increases more strongly with temperature than its formation rate from NO; it does
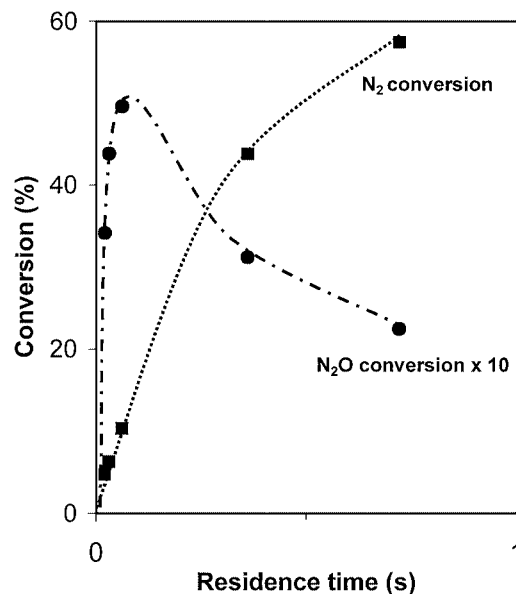
FIG. 1. Comparison of N_2 and N_2O conversion with varying residence time, 673 K, 1 kPa NO, Cu(0.60). Pretreated in He at 773 K for 2 h prior to the first NO exposure.

not exclude an intermediate role of N_2O at these higher temperatures.

On Cu(0.36), the apparent NO reaction order is 1.1 at 673 K and 1.5 at 873 K (Fig. 3). These noninteger values and their variation with temperature reflect a complex kinetic behavior inappropriate for power-law analysis. The reaction order in NO approaches a value of 2 as temperature increases. The expected decrease in the surface coverage
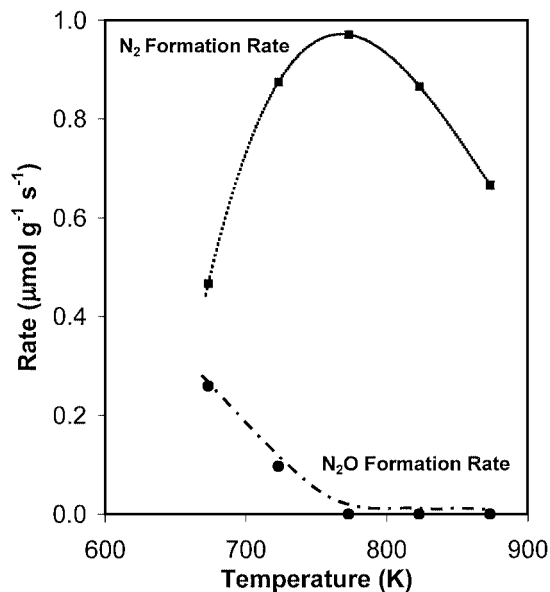
FIG. 2. N_2 formation and N_2O formation rates vs temperature for the catalyst Cu(0.58), with 1 kPa NO in the feed at contact time 0.031 s. Pretreated in He at 773 K for 2 h prior to the first NO exposure.
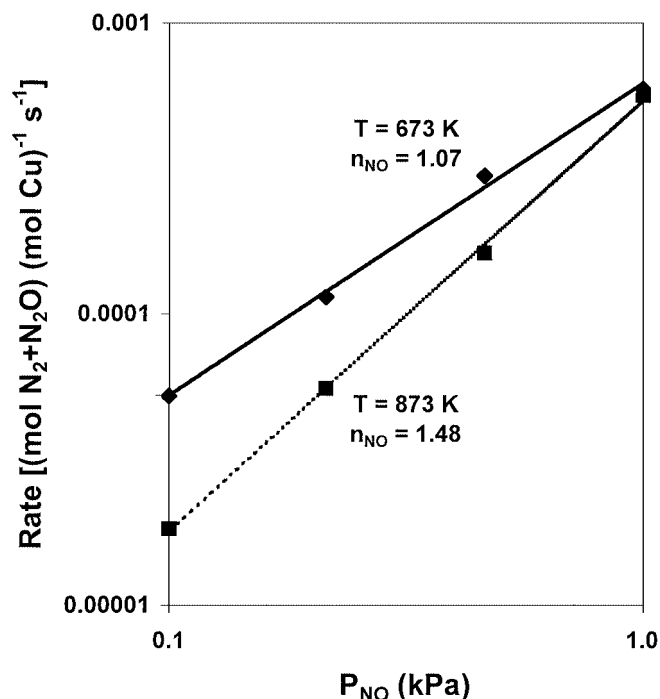
FIG. 3. Apparent order in NO (n_{NO}) measured on Cu(0.36) for 673 K (♦) and 873 K (■). Pretreated in He at 773 K for 2 h prior to the first NO exposure.

of all intermediates as temperature increases leads us to suggest that this behavior reflects bimolecular reactions of adsorbed NO on surfaces mostly free of adsorbed intermediates at high temperatures. The adsorbed NO molecules involved in these bimolecular pathways are likely to reside on a single site, such as two vicinal Cu^+ cations in sufficient proximity to form an oxygen bridge upon the decomposition of the two adsorbed NO and the desorption of N_2O (8, 9, 11).

NO_2 was detected in concentrations near those predicted by the thermodynamics for the $O + 1/2O_2 \rightleftarrows NO_2$ reaction on all Cu–ZSM5 catalysts at all reaction temperatures (Fig. 4). Thus, this reaction reaches quasiequilibrium within the catalyst bed. The extent of reaction is unaffected by any re-equilibration via homogeneous pathways within cooler heated transfer lines and analytical equipment after the reactor. NO_2 concentrations decreased sharply as temperature increased because of unfavorable thermodynamics; the equilibrium constant for this reaction decreases from 3.5 at 673 K, to 0.90 at 773 K, and to 0.32 at 873 K (3). The strong temperature dependence of the thermodynamic properties accounts for the slightly higher than equilibrium NO_2 concentrations detected in some cases. In all cases, however, the approach to equilibrium was independent of reactor residence time. In the absence of added O_2, NO_2 was only detected in substantial amounts below 723 K, and N_2 and O_2 were the predominant NO decomposition products at higher temperatures. N_2 and O_2 were detected in equimolar

amounts above 723 K, indicating the substantial absence of N_2O and NO_2 and the excellent N and O balances in these kinetic measurements.

The redox nature of NO decomposition reactions was probed by switching between pure He and NO-containing streams at a constant temperature; these experiments are described in detail and for a wider range of materials elsewhere (11). N_2 and O_2 formation rates during isothermal transients from pure He to 0.464% NO in He are shown in Fig. 5 for Cu(0.36) at 773 K, the temperature where the NO decomposition rates are the highest. Initial N_2 formation rates were very high, but they ultimately decreased to steady-state rates significantly lower than the maximum values reached during the early stages of the transient. O_2 formation rates were initially much lower than N_2 formation rates, but then increased to their equimolar steady-state values. The nitrogen surplus in the effluent indicates the net retention of some oxygen by Cu–ZSM5 during the initial stages of the transient. The resulting increase in oxygen surface concentration with time leads in turn to a smaller number of the reduced $\{Cu^+–\square–Cu^+\}$ centers required for NO adsorption and reaction. These data appear to confirm that NO decomposition on Cu–ZSM5 proceeds via a redox mechanism, in which N_2 and N_2O formation steps require reduced centers $\{Cu^+–\square–Cu^+\}$.

Figure 6 shows net oxygen desorption rates from samples pretreated in 50% O_2/He at 773 K for 2 h and then heated from ambient temperature to 1000 K using He or 0.464%
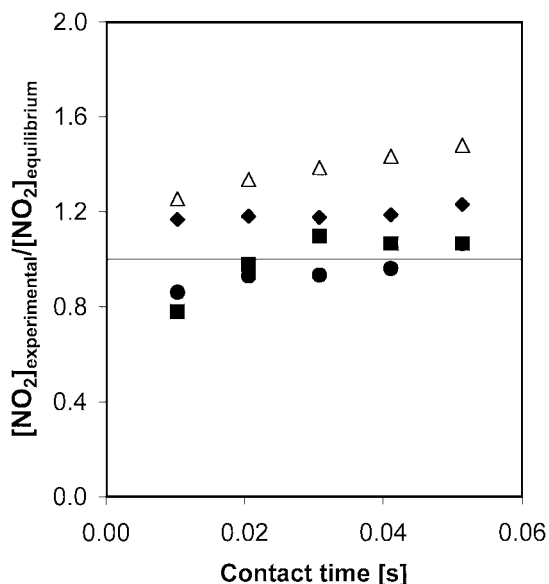
FIG. 4. Comparison of measured NO_2 concentration for Cu(0.58) and NO_2 concentration calculated from the equilibrium constant for $NO + \frac{1}{2}O_2 \rightleftarrows NO_2$ (evaluated at each temperature) and the NO and O_2 concentrations. △, 673 K, with 0.6 kPa NO and 0.215 kPa O_2; ♦, 723 K, with 0.6 kPa NO and 0.215 kPa O_2; ●, 773 K, with 0.6 kPa NO and 1.0 kPa O_2; ■, 823 K, with 0.6 kPa NO and 1.0 kPa O_2, with varying residence time.
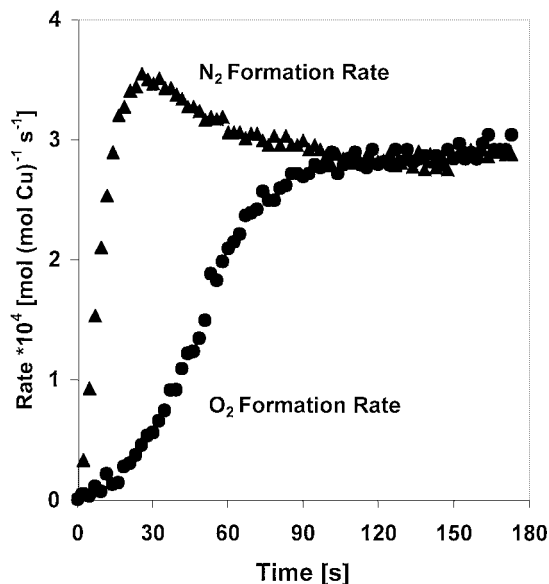
FIG. 5. Isothermal transient to follow the NO decomposition on Cu–ZSM5, Cu(0.36), switch from He to 0.464 kPa NO/He at 773 K. Pretreated in He at 773 K for 2 h prior to the first NO exposure.

NO/He as the carrier gas (11). Net oxygen desorption rates in the presence of NO were measured from an oxygen atom balance in the effluent gas (Eq. [1]):

$$r_{O,ads} = r_{N,tot} - r_{O,tot} = 2r_{N_2} + r_{N_2O} - 2r_{O_2} - r_{NO_2}. \quad [1]$$

Preadsorbed oxygen desorbs at lower temperatures when NO is present in the gas phase than when pure He is
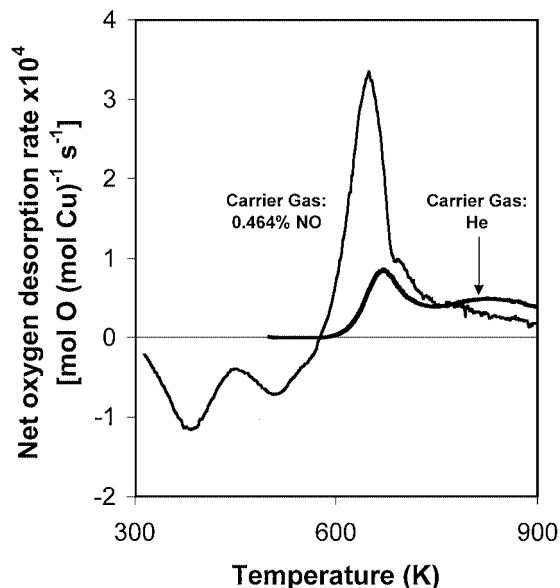
used (Fig. 6). This suggests the involvement of NO-derived species or of gas-phase NO, and not just adsorbed oxygen, in the steps required for removing the oxygen species formed in NO decomposition as O_2. The equilibrium NO_2 concentrations achieved at all reaction conditions (Fig. 4) require that the reaction of NO with adsorbed oxygen and its reverse reaction—NO_2 decomposition—proceed more rapidly than NO decomposition. The equilibrated formation of NO_2 guarantees the presence and the rapid nature of a set of elementary steps that ensures kinetic communication among oxygens residing at distant dimer sites via the formation, desorption, and gas-phase diffusion of NO_2. These distant oxygen atoms would otherwise require oxygen atom migration for recombinative desorption steps to occur at steady-state rates commensurate with the rate of formation of these oxygen species during NO decomposition.

Infrared studies during NO decomposition have detected a nitrate species bridging two Cu atoms as the most abundant nitrogen-containing species chemisorbed on Cu–ZSM5 at low temperatures (<673 K) (20–22). These species have been proposed as intermediates in O_2 formation during NO decomposition; in temperature-programmed desorption studies of preadsorbed NO, these nitrate species decompose to NO and O_2 (11, 41), thus re-forming the NO molecule used as the mobile oxygen shuttle that allows efficient kinetic communication among Cu dimer sites.

Several adsorbed species coexist during NO decomposition (8, 17, 20). The most abundant among them are shown in Scheme 1.

For some of these species, such as NO_2^*, NO_3^*, and O_2^*, structures other than those shown are possible for the stoichiometry shown. We have assigned a formal 2-charge to adsorbed NO_2 and NO_3 species in order to maintain

FIG. 6. Net oxygen desorption rate from Cu(0.58), for samples treated in 50% O_2/He at 773 K for 2 h. The temperature was ramped from 298 to 900 K at 0.167 K s^{-1} using either He or 0.464 kPa NO/He as the carrier gas.
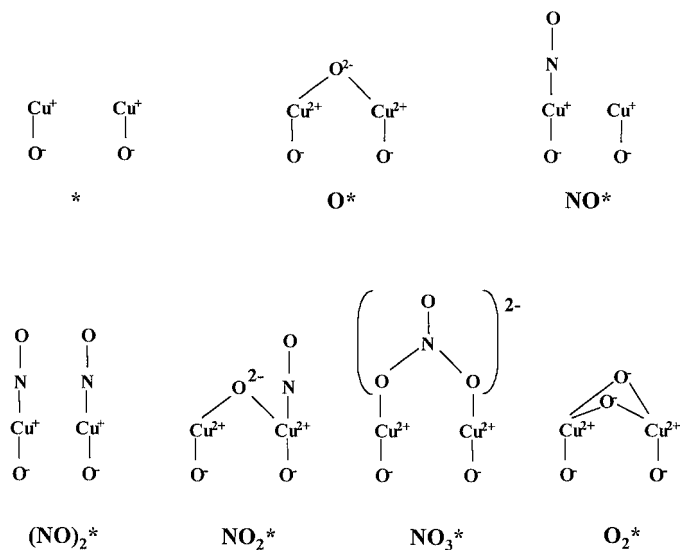
SCHEME 1

TABLE 2

Mechanism for NO Decomposition on Cu–ZSM5

NO activation and N_2O and N_2 formation

1.	$* + NO \rightleftarrows NO^*$	(quasiequilibrated)
2.	$NO^* + NO \rightleftarrows (NO)_2^*$	(quasiequilibrated)
3.	$(NO)_2^* \rightarrow O^* + N_2O$	
4.	$* + N_2O \rightleftarrows N_2O^*$	(quasiequilibrated)
5.	$N_2O^* \rightarrow O^* + N_2$	

O_2 formation

6.	$O^* + NO \rightleftarrows NO_2^*$	(quasiequilibrated)
7.	$NO_2^* \rightleftarrows * + NO_2$	(quasiequilibrated)
8.	$O^* + NO_2 \rightleftarrows NO_3^*$	(quasiequilibrated)
9.	$NO_3^* \rightleftarrows O_2^* + NO$	(quasiequilibrated)
10.	$O_2^* \rightleftarrows * + O_2$	(quasiequilibrated)

Note. Steps $1–5 : 2* + 2NO \rightarrow 2O^* + N_2$ (N_2 formation).
Steps $6–10 : 2O^* \rightleftarrows 2* + O_2$ (O_2 formation).
Steps $1–10 : 2NO \rightarrow N_2 + O_2$ (overall reaction).

charge neutrality for all exchanged Cu^{2+} species, but the validity of this assignment or the actual electron distribution between the adsorbed species and the Cu atoms do not influence the kinetic treatment or the mechanistic conclusions of this study, for which only stoichiometry, and not molecular structure or charge, is relevant.

The results presented above led us to propose an NO decomposition mechanism (Table 2) that is consistent with the adsorbed species detected by infrared (8, 17, 20) and with transient reduction and reaction studies (10, 11) on Cu–ZSM5. The equilibrium between NO, O_2, and NO_2 guarantees the quasiequilibrated nature of oxygen removal steps via steps 6–10 (Table 2) during catalytic NO decomposition. The proposed steps, many of them elementary in nature, are listed in Table 2 and shown as a catalytic cycle in Fig. 7.

Steady-state rate measurements cannot discern the relative kinetic relevance of steps 2 and 3, because the resulting rate equations (but not the meaning of the lumped apparent rate constant) are identical when either step 2 or 3 is quasiequilibrated. In both cases, NO concentration appears as $[NO]^2$ in the numerator of the rate expression. In the sequence shown in Table 2, the initial irreversible formation of N_2O determines overall NO decomposition rates. The subsequent N_2O decomposition steps influence N_2 selectivity, but not NO decomposition rates. Thus, the overall NO molar decomposition rate is given by twice the combined molar formation rates of N_2O and N_2.

NO acts in the proposed mechanism as an oxygen transfer agent, which allows efficient kinetic communication among distant oxygen atoms and the formation of O_2 without requiring surface or gas-phase diffusion of oxygen atoms at distant Cu dimers. The equilibrated nature of the catalytic oxidation of NO to NO_2 using O_2 ensures that this O_2 formation pathway is not only available during NO decomposition, but also much faster than NO decomposition turnovers. NO reacts with O^* to form NO_2, which desorbs,

diffuses in the gas phase, and either decomposes back to NO and O^* at a reduced center ($*$) or reacts with another O^* at a remote dimer to form (NO_3^*). These nitrate species (NO_3^*) have been detected by infrared studies during NO decomposition (20).

NO acts in steps 6 and 7 (Table 2) as a reducing agent, in a manner reminiscent of the role of other reductants, such as CO and NH_3, in NO reduction reactions (1, 2). In NO reduction by CO, the thermodynamic stability of the CO_2 formed causes the oxygen atoms formed in NO decomposition to leave the reaction zone as CO_2. In NO decomposition, however, the oxygen carrier (NO_2) is unstable, and it decomposes to NO and O_2 within the reactor; as a result, at least one NO molecule undergoes a reversible oxidation–reduction cycle during each NO decomposition turnover. The steps involved in the decomposition of NO_3^* into $*$, NO, and O_2 occur concurrently (steps 9 and 10), because NO and O_2 evolve simultaneously and in close to equimolar amounts at 660 K during the decomposition of preadsorbed NO on Cu–ZSM5 (11). During NO decomposition, the O^* concentration is determined by the thermodynamics for the overall $2O^* \rightleftarrows O_2 + 2*$ reaction, irrespective of the mechanism by which this net reaction proceeds. As a result, the direct recombinative desorption and the proposed pathways (steps 6–10, Table 2) lead to identical O^* coverages, but the NO-mediated O_2 formation pathways are significantly faster and provide the kinetic route to this equilibrium during NO decomposition on Cu–ZSM5.

NO Decomposition Kinetic Rate Equations

The sequence of elementary steps shown in Table 2 and in Fig. 7 can be used to obtain a rate expression by using the pseudo-steady-state approximation for all adsorbed species and quasiequilibrium assumptions for some of the reaction
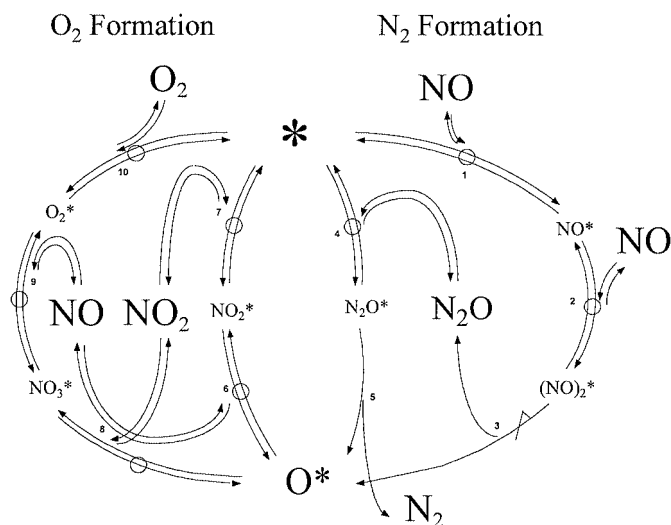
FIG. 7.   Catalytic cycle for NO decomposition on Cu–ZSM5 catalysts.

steps. In what follows, equilibrium constants are denoted as K_i and rate constants as k_i. The quasiequilibrated step 1 related [NO*] to [*] and [NO] (Eq. [2]):

$$[NO^*] = K_1[NO][*]. \qquad [2]$$

If step 2 is quasiequilibrated, after using Eq. [2] to eliminate [NO*] we obtain

$$[(NO)_2^*] = K_2[NO][NO^*] = K_1 K_2[NO]^2[*]. \qquad [3]$$

Then, the reaction rate (defined as the sum of the N_2 and N_2O formation rates) is determined by the rate of $(NO)_2^*$ decomposition in step 3:

$$r_3 = k_3[(NO)_2^*] = k_3 K_1 K_2[NO]^2[*]. \qquad [4]$$

A site balance for all active sites $[L]$ contains terms for [*], [O*], [NO*], [O$_2^*$], [NO$_3^*$], and [NO$_2^*$]:

$$[L] = [*] + [NO^*] + [O^*] + [O_2^*] + [NO_3^*] + [NO_2^*]. \qquad [5]$$

$[(NO)_2^*]$ and $[N_2O^*]$ were not detectable as a denominator term in any of the acceptable rate equations or as adsorbed species in infrared studies during the reaction (20). An overall equilibrium constant K_α is defined (Eq. [6]) for quasiequilibrated steps 6–10. This sequence of steps yields an expression of [O*] in terms of free sites [*] and [O$_2$] concentrations:

$$K_\alpha = (K_6 K_7 K_8 K_9 K_{10})^{-1/2}, \qquad [6]$$

$$[O^*] = K_\alpha[O_2]^{1/2}[*]. \qquad [7]$$

Similarly, [O$_2^*$], [NO$_3^*$], and [NO$_2^*$] can be obtained in terms of [*]

$$[O_2^*] = K_{10}^{-1}[O_2][*], \qquad [8]$$

$$[NO_3^*] = K_9^{-1}[NO][O_2^*] = K_\beta[NO][O_2][*]$$
$$(K_\beta = K_9^{-1}K_{10}^{-1}), \qquad [9]$$

$$[NO_2^*] = K_6 K_\alpha[NO][O_2]^{1/2}[*]. \qquad [10]$$

Equations [2] and [7]–[10] contain the concentrations of all abundant species in terms of the concentration of reduced dimers [*], which can then be substituted into Eq. [5] to obtain an expression for [*] in terms of $[L]$:

$$[L] = [*](1 + K_1[NO] + K_\alpha[O_2]^{1/2} + K_{10}^{-1}[O_2]$$
$$+ K_\beta[NO][O_2] + K_6 K_\alpha[NO][O_2]^{1/2}). \qquad [11]$$

This expression can be solved for [*] and introduced into Eq. [4] in order to obtain a rate equation in terms of reactants and product concentrations and of the number of
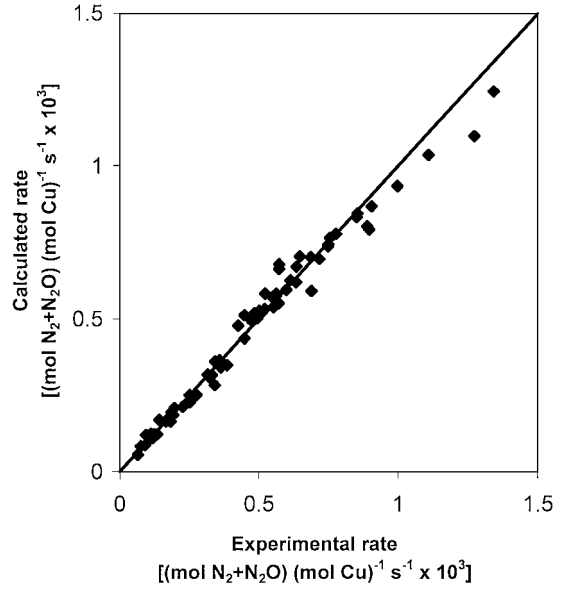
FIG. 8. Parity plots for the rate expression with * and O* terms. The rate data were obtained for a range of temperatures from 723 to 823 K for Cu(0.58).

catalytic sites $[L]$:

$$r = \frac{k_3 K_1 K_2[NO]^2[L]}{1 + K_1[NO] + K_\alpha[O_2]^{1/2} + K_{10}^{-1}[O_2] + K_\beta[NO][O_2] + K_6 K_\alpha[NO][O_2]^{1/2}}. \qquad [12]$$

We note that reduced and oxidized Cu dimers are intermediates in NO decomposition and that it would be inappropriate to describe one or the other as the catalytic site; they represent oxidation states of the Cu centers when the active sites are "occupied" or "unoccupied."

Steady-state NO decomposition rate data as a function of NO (0.2–0.6 kPa) and O_2 (0–1 kPa) at three temperatures are compared with the rate equation obtained from the elementary steps 1–10 (Eq. [12]) in Fig. 8. This comparison illustrates the consistency among the proposed mechanism, the expected most abundant surface species (*masi* (42)), and the measured kinetic rate data. Rate equations with second-order NO dependencies were required for accurate descriptions of experimental NO decomposition rates at all temperatures. At 723 K and higher temperatures only the $[O_2]^{1/2}$ term in the denominator was required, giving a rate equation of the form (Eq. [13])

$$r = \frac{k_{app}[NO]^2}{1 + K_\alpha[O_2]^{1/2}}, \qquad [13]$$

consistent with O* and * as *masi*. Denominator terms corresponding to NO*, NO$_2^*$, or NO$_3^*$ concentrations were not required in order to describe reaction rates at 723 K or higher temperatures. Infrared (20) and transient desorption (11) studies have shown that NO$_3^*$ decomposes at ~673 K and

NO* desorbs also at ~673 K (11), in agreement with the proposal of O* and * as *masi* species at temperatures above 700 K. The excellent agreement between predicted and experimental rates is illustrated in Fig. 8 for all kinetic data at temperatures between 723 and 823 K.

Below 723 K, the regression analysis is less conclusive about the identity of the *masi* species. At 673 K, a rate equation containing denominator terms for NO^*, O_2^*, O^*, and * gave the lowest value of the relative error, but neither NO^* nor O_2^* have been detected by infrared studies during catalytic NO decomposition at these temperatures. A rate equation with NO_3^*, O^*, and * denominator terms (Eq. [14]) gave only a slightly larger error than the equation containing also terms for NO^*, O_2^*, O^*, and *. We consider the presence of NO_3^*, O^*, and * as *masi* a more realistic representation of the situation and of the rate data:

$$r = \frac{k_{app}[NO]^2}{1 + K_\alpha[O_2]^{1/2} + K_\beta[NO][O_2]}. \quad [14]$$

This assessment is based on the detection of NO_3^* as the most abundant infrared-active adsorbed species (20) and on the lack of experimental or theoretical support for significant O_2^* concentrations during reaction or during oxidative treatments of these samples.

Some of the features in Table 2 resemble those proposed for NO decomposition on Ba/MgO (29), $La_{0.8}Sr_{0.2}CoO_3$ and $La_{0.4}Sr_{0.6}Mn_{0.8}Ni_{0.2}O_3$ (30), and Mn_2O_3 and Mn_3O_4 (31). These studies also found a second-order NO concentration dependence, which was attributed to a quasiequilibrated first NO adsorption step. On supported Pt and on unsupported Ni, Fe, Co, and Zr catalysts, NO decomposition rates were found to be first-order in NO (26–28). The molecular adsorption of NO was proposed as the kinetically relevant step on Pt (26–28), even though molecular adsorption is typically fast and nonactivated. All these studies reported inhibition of NO decomposition rates by O_2 through quasiequilibrated adsorption–desorption steps, but the proposed pathways for oxygen desorption steps differ among these studies. On metal oxide catalysts, recombinative desorption of lattice oxygen atoms was proposed (29). In contrast with the similar proposal for Cu–ZSM5, there are no reasonable objections to this proposal for metal oxides, which contain a high density of vicinal lattice oxygens and significant lattice oxygen mobility. The first-order dependence of O_2 in the denominator, found on Pt (26–28) and on perovskite-type catalysts (30), differ from the $[O_2]^{0.5}$ dependence observed on Cu–ZSM5 catalysts and it cannot be reconciled with quasiequilibrated dissociative oxygen adsorption–desorption steps.

Li and Hall reported that NO decomposition rates were proportional to $[NO]^{1.0}$ and $[O_2]^{-0.5}$ on Cu–ZSM5 (34). This NO dependence differs from that reported here; this difference appears to reflect the power-law analysis and the higher NO partial pressures used in the earlier study

(1–4 kPa vs 0.1–1 kPa). For a given NO conversion, the O_2 concentration is higher and the $[O_2]^{0.5}$ denominator term becomes increasingly dominant as the NO pressure increases. Thus, as NO pressures increase, the proportional increase in O_2 concentration leads to the partial cancellation of the $[NO]^2$ numerator term. In our study, these changes in O_2 concentrations were explicitly considered in the well-mixed integral reactor analysis used for all kinetic data. The present study also differs from the previous studies in the mechanism proposed for O_2 formation. In our study, the recombinative desorption of O^* is replaced by a sequence of steps that does not require atomic contact among O^* sites. This sequence involves the sequential formation of NO_2^*, NO_2, and NO_3^*; its quasiequilibrium during NO decomposition is assured by the $NO/NO_2/O_2$ equilibrium observed at all reaction conditions on Cu–ZSM5.

Temperature Dependence of the Rate Constants and the Equilibrium Constants in Rate Equations

Steady-state NO decomposition rates on Cu–ZSM5 show an unusual temperature dependence, characterized by a normal Arrhenius behavior up to ~773 K followed by a decrease in rates at higher temperatures (4, 5, 34). These rate changes are reversible during temperature cycling; they represent true kinetic effects and not deactivation or structural changes of active Cu centers at high temperatures. Typical Arrhenius plots for NO decomposition rates are shown in Fig. 9 at various NO and O_2 pressures on Cu(0.58),
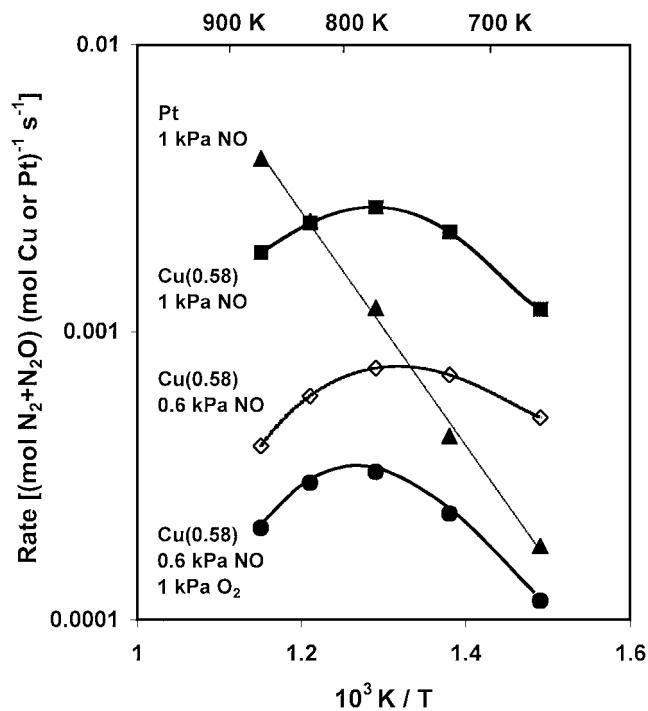
FIG. 9. Arrhenius plots for various NO and O_2 partial pressures. ▲, 1 kPa NO on Pt/Al$_2$O$_3$; ■, 1 kPa NO on Cu(0.58); ◇, 0.6 kPa NO on Cu(0.58); ●, 0.6 kPa NO and 1 kPa O_2 on Cu(0.58).

together with rates measured on Pt/Al_2O_3. All Cu–ZSM5 samples in this study showed similar temperature trends, and NO decomposition rates reached maximum values at ~773 K for 1 kPa NO. In contrast, NO decomposition on Pt/Al_2O_3 showed normal Arrhenius behavior at 673–873 K, with an apparent activation energy of 18 kcal/mol, which agrees with the value of 18.4 kcal/mol reported previously (26). On Cu–ZSM5, the temperature at which maximum NO decomposition rates occur varies with NO and O_2 partial pressures. At a given NO partial pressure (0.6 kPa), the rate maximum shifts from ~753 to ~793 K when 1 kPa O_2 is added to a stream containing only NO reactants. The temperature required for maximum NO decomposition rates is slightly higher for 1 kPa NO (~773 K) than for 0.6 kPa NO (~753 K).

This unusual temperature effect led us to examine the effects of temperature on individual rate parameters (k_{app} and K_α), which were separated into their elementary step rate and equilibrium constants. This approach allows us to assign specific temperature dependences for elementary steps and the effects of temperature and of gas-phase concentrations on the relative coverage of reactive intermediates. The apparent rate constant k_{app} reflects the kinetic and thermodynamic behavior of several elementary steps. Without loss of generality, we consider both NO adsorption steps (steps 1 and 2 in Table 2) to be quasiequilibrated, which makes step 3 the kinetically relevant step in the overall sequence in Table 2. All rate and equilibrium constants (K_1, K_2, and k_3) are of Arrhenius form and they appear in the apparent rate constants (k_{app}) as

$$k_{app} = A_{app}e^{-E_{app}/RT}, \quad [15]$$

$$k_{app} = K_1K_2k_3[L], \quad [16]$$

$$K_1 = \frac{A_{a,1}}{A_{d,1}}e^{\Delta Q_1/RT} = \frac{A_{a,1}}{A_{d,1}}e^{-\Delta H_1/RT}, \quad [17]$$

$$K_2 = \frac{A_{a,2}}{A_{d,2}}e^{\Delta Q_2/RT} = \frac{A_{a,2}}{A_{d,2}}e^{-\Delta H_2/RT}, \quad [18]$$

$$k_3 = A_3e^{-E_{a,3}/RT}. \quad [19]$$

The apparent activation energy is obtained from the slope in the Arrhenius plot where ($\ln k_{app}$) is plotted against the reciprocal temperature (Eq. [20]). This apparent activation energy contains the adsorption enthalpies for adsorption steps 1 and 2 and the activation energy for step 3:

$$\ln k_{app} = \ln A_{app} - \frac{E_{a,app}}{RT}$$
$$= \ln\left(\frac{A_{a,1}}{A_{d,1}}\right) + \ln\left(\frac{A_{a,2}}{A_{d,2}}\right) + \ln A_3 + \ln[L]$$
$$- \left(\frac{\Delta H_1 + \Delta H_2 + E_{a,3}}{RT}\right), \quad [20]$$

$$E_{app} = E_{a,3} + \Delta H_1 + \Delta H_2. \quad [21]$$
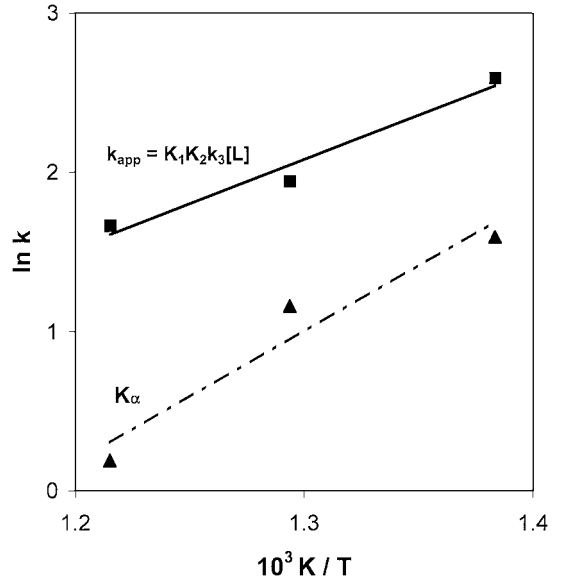
FIG. 10. Arrhenius plot for the parameters k_{app} and K_α obtained from the regression for Cu(0.58).

The equilibrium constant for O_2 adsorption, K_α is given by

$$K_\alpha = \frac{A_{a,\alpha}}{A_{d,\alpha}}e^{\Delta Q_a/RT} = \frac{A_{a,\alpha}}{A_{d,\alpha}}e^{-\Delta H_a/RT}. \quad [22]$$

From the regression analysis presented earlier (Fig. 8 and Eq. [13]), we obtained k_{app} and K_α at various temperatures (723, 773, and 823 K). An Arrhenius plot of these parameters is shown in Fig. 10. Both k_{app} and K_α decreased with increasing temperature, with K_α showing the stronger temperature dependence. These data give values of −11 kcal/mol for $E_{a,app}$ and −18 kcal/mol for ΔH_α.

The observed negative apparent activation energy requires that the activation energy for the kinetically relevant step 3 be smaller than the sum of the heats of adsorption for the two preequilibrated adsorption steps (1 and 2). The low activation energy for step 3 is evident from the formation of N_2O near room temperature during the initial transient exposure of Cu–ZSM5 samples to NO (11). NO adsorption steps are likely to be exothermic, as is the case for most chemisorption processes, and their thermodynamics become unfavorable with increasing temperature. These data suggest that NO adsorption equilibrium constants (K_1 and K_2) decrease more strongly with temperature than k_3 increases, leading to an overall decrease in k_{app} with increasing temperature (Fig. 10). The decrease in K_α with increasing temperature shows that K_α represents an exothermic net reaction. This is consistent with expected exothermic nature of the net O_2 adsorption process described by the combination of elementary steps leading to K_α. The observed temperature behavior of K_α is also consistent with the observed increase in reduced Cu dimers with increasing temperature (10, 11).
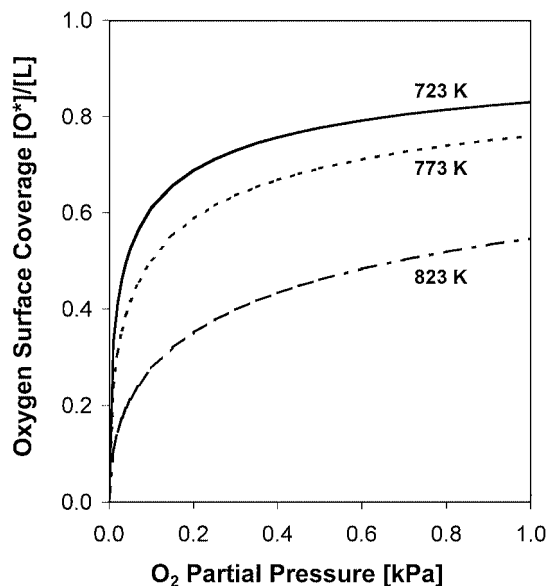
FIG. 11. Calculated oxygen surface coverage ($[O^*]/[L]$) vs partial pressure of O_2 on Cu(0.58).

From these values of K_α and the gas-phase O_2 concentration, fractional $[O^*]$ surface coverages can be obtained, using denominator terms in the rate expression valid at 723 K and above (Eq. [13]). The oxygen fractional coverage ($[O^*]/[L]$) is plotted as a function of O_2 partial pressure in Fig. 11 at 723, 773, and 823 K. At low temperatures and high O_2 partial pressures, the oxygen fractional coverage approaches unity and O^* becomes the *masi* during NO decomposition. At higher temperature and lower O_2 partial pressures, the oxygen coverage decreases and free sites (*) become the *masi*.

Combining the temperature dependence of these parameters and the O^* surface coverage, we return to the rate expression (Eq. [13]) in order to describe how NO decomposition rates change with temperature at various gas-phase compositions (shown in Fig. 9):

$$r = \frac{k_{\text{app}}[NO]^2}{1 + K_\alpha[O_2]^{1/2}} \quad (k_{\text{app}} = K_1 K_2 k_3 [L]). \quad [13]$$

At low temperatures, the $K_\alpha[O_2]^{1/2}$ term in the denominator of Eq. [13] becomes larger than 1, and the rate approaches an expression of the form

$$r = \frac{k_{\text{app}}[NO]^2}{K_\alpha[O_2]^{1/2}}. \quad [23]$$

For this rate expression, the overall rate constant is k_{app}/K_α, which increases with increasing temperature. This leads to an increase in the NO decomposition rate with increasing temperature and to a positive apparent activation energy as long as O^* remains the *masi*. At temperatures below $\sim$723 K, NO_3^* is present in substantial amounts along with

the most abundant O^*, but at 723 K and above its concentration is negligible compared to * and O^*. This adds an extra denominator term below 723 K, with an equilibrium constant corresponding to an exothermic reaction; it behaves with temperature similarly to the term for O^*, and it is not included in order to simplify the arguments without loss of generality. As the temperature increases, $K_\alpha[O_2]^{1/2}$ and the other denominator terms decrease, leaving * as the *masi*, and Eq. [13] approaches

$$r = k_{\text{app}}[NO]^2 \quad [24]$$

as O_2 desorption is favored and * becomes the *masi* species. At temperatures above 773 K, for which the O^* term in the denominator of Eq. [13] becomes smaller with increasing temperature, k_{app} becomes the overall rate constant for the NO decomposition reaction; it then acquires a negative apparent activation energy. This change in *masi* from O^* to * as temperature increases causes the observed change in apparent activation energy and the maximum in NO decomposition rates at intermediate temperatures (Fig. 9).

The shift in the temperature at which the rate reaches a maximum value for different gas-phase compositions can be explained in terms of these changes in the identity of the *masi* with increasing temperature. High O_2 partial pressures cause the shift in the *masi* from O^* to * to occur at higher temperatures; as a result, the temperature required to reach maximum NO decomposition rate would increase (Fig. 9). The temperature required for maximum rates is indeed higher at 1 kPa O_2 (793 K) than when O_2 is not added (753 K). Also, this temperature is higher at 1 kPa NO (773 K) than at 0.6 kPa NO (753 K), because higher O^* concentrations are present at the higher O_2 concentrations prevalent during decomposition of higher concentrations of NO. These data and their mechanistic implications suggest that unfavorable NO adsorption thermodynamics lead to the observed decrease in NO decomposition rates at high temperatures.

This study illustrates the mechanistic complexity of the stoichiometrically simple NO decomposition reaction, as well as the role of NO as both a reductant and an oxidant in catalytic turnovers. The proposed sequence of steps (Table 2) is consistent with transient (11) and infrared (17, 20), studies, and it includes pathways for the formation and reaction of N_2O and NO_2 as gas-phase intermediates in the formation of N_2 and O_2 as the ultimate NO decomposition products.

CONCLUSIONS

Steady-state and transient NO decomposition data were used to infer a set of elementary steps for the formation of N_2O, NO_2, N_2, and O_2 during NO decomposition on Cu–ZSM5. The adsorbed species and Cu structures involved in these elementary steps are consistent with previous

spectroscopic evidence. N_2O was the initial product of NO decomposition and the adsorption of both NO and N_2O required reduced Cu dimers $\{Cu^+–\square–Cu^+\}^{2+}$ formed by the removal of a bridging oxygen from vicinal Cu^{2+} species at exchange sites $\{Cu^{2+}–O^{2-}–Cu^{2+}\}^{2+}$. The redox nature of the NO and N_2O decomposition pathways was confirmed by transient kinetic measurements, which showed the net incorporation of oxygen and a concomitant decrease in reaction rates as decomposition proceeded on Cu–ZSM5 samples containing reduced Cu^+ dimers. The reaction of two NO molecules adsorbed on vicinal Cu atoms led to N_2O formation at room temperature, suggesting that the activation energy for this bimolecular reaction is very small. The significant heat of adsorption of NO on Cu^+ dimers, and the transition from $\{Cu^{2+}–O^{2-}–Cu^{2+}\}^{2+}$ to $\{Cu^+–\square–Cu^+\}^{2+}$ as the predominant Cu species, causes the observed decrease in NO decomposition rates above temperatures higher than $\sim$750 K.

The communication between O_2 and oxygen adsorbed as bridged species on Cu dimers is mediated by rapid and reversible NO oxidation and NO_2 decomposition reactions, which allow reactions between remote adsorbed oxygen species via migration of NO_2 in the gas-phase instead of adsorbed oxygen on the zeolite surface. In these steps, the decomposition of an adsorbed nitrate species leads to the evolution of O_2 molecules and to the regeneration of the NO molecules used to carry oxygen via the gas phase as NO_2. These pathways were confirmed by the equilibrium NO_2 concentrations measured at all conditions during NO decomposition on Cu–ZSM5. These O_2 formation pathways avoid the need for vicinal oxygen atoms and for recombinative desorption steps; they suggest that NO acts both as an oxidant and as a recyclable reductant during its catalytic decomposition on Cu–ZSM5.

The mechanism proposed is consistent with the steady-state kinetic data and leads to reasonable values and temperature dependences for all rate parameters. The relative abundance of various surface species inferred from this rate equation is consistent with independent spectroscopic studies of adsorbed species and of Cu structures. The superior activity of Cu–ZSM5 samples in NO decomposition reactions reflects the availability of two-electron redox cycles without requiring the reduction of Cu^{2+} beyond Cu^+ by using a Cu^{2+} dimer to accommodate a two-electron reduction process without the formation (and agglomeration) of Cu metal. In addition, the labile nature of the bridged oxygen ligands in oxidized Cu dimers and the balanced equilibrium between their oxidized $\{Cu^{2+}–O^{2-}–Cu^{2+}\}^{2+}$ and reduced $\{Cu^+–\square–Cu^+\}^{2+}$ states allow the redox cycles required as part of each NO decomposition turnover to occur rapidly.

ACKNOWLEDGMENTS

REFERENCES

1. Topsoe, N.-Y., *Cattech* **1**, 125 (1997).
2. Nakajima, F., *Catal. Today* **10**, 1 (1991).
3. Stull, D. R., Westrum, E. F., Jr., and Sinke, G. C., "The Chemical Thermodynamics of Organic Compounds." Krieger, Malabar, FL, 1987.
4. Iwamoto, M., Furukawa, H., Mine, Y., Uemura, F., Mikuriya, S., and Kagawa, S., *J. Chem. Soc. Chem. Commun.* **16**, 1272 (1986).
5. Iwamoto, M., Yahiro, H., Mine, Y., and Kagawa, S., *Chem. Lett.* **2**, 213 (1989).
6. Iwamoto, M., *Catal. Today* **10**, 57 (1991).
7. Iwamoto, M., Yahiro, H., Tanda, K., Mizuno, N., Mine, Y., and Kagawa, S., *J. Phys. Chem.* **95**, 3727 (1991).
8. Iwamoto, M., Yahiro, H., Mizuno, N., Zhang, W. X., Mine, Y., Furukawa, H., and Kagawa, S., *J. Phys. Chem.* **96**, 9360 (1992).
9. Beutel, T., Sarkany, J., Lei, G. D., Yan, J. Y., and Sachtler, W. M. H., *J. Phys. Chem.* **100**, 845 (1996).
10. Da Costa, P., Moden, B., Meitzner, G., Lee, D. K., and Iglesia, E., submitted for publication.
11. Moden, B., Da Costa, P., Lee, D. K., and Iglesia, E., submitted for publication.
12. Liu, D. J., and Robota, H. J., *Catal. Lett.* **21**, 291 (1993).
13. Giamello, E., Murphy, D., Magnacca, G., Shioya, Y., Nomura, T., and Anpo, M., *J. Catal.* **136**, 510 (1992).
14. Valyon, J., and Hall, W. K., *J. Phys. Chem.* **97**, 1204 (1993).
15. Spoto, G., Zecchina, A., Bordiga, S., Ricchiardi, G., Martra, G., Leofanti, G., and Petrini, G., *Appl. Catal. B* **3**, 151 (1994).
16. Lei, G. D., Adelman, B. J., Sarkany, J., and Sachtler, W. M. H., *Appl. Catal. B* **5**, 245 (1995).
17. Aylor, A. W., Larsen, S. C., Reimer, J. A., and Bell, A. T., *J. Catal.* **157**, 592 (1995).
18. Jang, H. J., Hall, W. K., and d'Itri, J. L., *J. Phys. Chem.* **100**, 9416 (1996).
19. Schay, Z., Knozinger, H., Guczi, L., and Pal-Borbely, G., *Appl. Catal. B.* **18**, 263 (1998).
20. Konduru, M. V., and Chuang, S. S. C., *J. Phys. Chem. B* **103**, 5802 (1999).
21. Konduru, M. V., and Chuang, S. S. C., *J. Catal.* **187**, 436 (1999).
22. Konduru, M. V., and Chuang, S. S. C., *J. Catal.* **196**, 271 (2000).
23. Park, S.-K., Kurshey, V., Luan, Z., Lee, C. V., and Kevan, L., *Microporous Mesoporous Mater.* **38**, 255 (2000).
24. Sarkany, J., d'Itri, J. L., and Sachtler, W. M. H., *Catal. Lett.* **16**, 241 (1992).
25. Hightower, J. W., and van Leirsburg, D. A., *in* "The Catalytic Chemistry of Nitrogen Oxides" (R. L. Klimisch and J. G. Larson, Eds.), p. 63. Plenum, New York, 1975.
26. Amirnazmi, A., Benson, J. E., and Boudart, M., *J. Catal.* **30**, 55 (1973).
27. Amirnazmi, A., and Boudart, M., *J. Catal.* **39**, 383 (1975).
28. Lim, K. J., Loffler, D. G., and Boudart, M., *J. Catal.* **100**, 158 (1986).
29. Xie, S. B., Rosynek, M. P., and Lunsford, J. H., *J. Catal.* **188**, 24 (1999).
30. Teraoka, Y., Harada, T., and Kagawa, S., *J. Chem. Soc. Faraday Trans.* **94**, 1887 (1998).
31. Yamashita, T., and Vannice, A., *J. Catal.* **163**, 158 (1996).

32. Winter, E. R. S., *J. Catal.* **22**, 158 (1971).
33. Li, Y., and Hall, W. K., *J. Phys. Chem.* **94**, 6145 (1990).
34. Li, Y., and Hall, W. K., *J. Catal.* **129**, 202 (1991).
35. Campa, M. C., Indovina, V., Minelli, G., Moretti, G., Pettiti, I., Porta, P., and Riccio, A., *Catal. Lett.* **23**, 141 (1994).
36. Zhang, Y., Lee, K. M., Sarofim, A. F., Hu, Z. C., and Flytzani-Stephanopoulos, M., *Catal. Lett.* **31**, 75 (1995).
37. Schay, Z., and Guczi, L., *Catal. Today* **17**, 175 (1993).
38. Froment, G. F., and Bischoff, K. B., "Chemical Reactor Analysis and Design," 2nd ed. Wiley, New York, 1990.
39. Donati, G., and Buzzi-Ferraris, G., *Chem. Eng. Sci.* **29**, 1504 (1974).
40. Villa, P. L., Forzatti, P., Buzzi-Ferraris, G., Garone, G., and Pasquon, I., *Ind. Eng. Chem. Prod. Res. Dev.* **24**, 12 (1985).
41. Li, Y., and Armor, J. N., *Appl. Catal.* **76**, L1 (1991).
42. Boudart, M., and Djega-Mariadassou, G., "Kinetics of Heterogeneous Catalytic Reactions." Princeton University Press, Princeton, NJ, 1984.